Ram Accelerator Barrel Response to Transient Loads

Nathan Wagner

A thesis

submitted in partial fulfillment of the

requirements for the degree of

Master of Science in Aeronautics and Astronautics

University of Washington

2024

Committee:

Carl Knowlen

Brian Leege

Program Authorized to Offer Degree:

Aeronautics and Astronautics

©Copyright 2024

Nathan Wagner

University of Washington

Abstract

Ram Accelerator Barrel Response to Transient Loads

Nathan Wagner

Chair of the Supervisory Committee:

Carl Knowlen

Department of Aeronautics and Astronautics

The ram accelerator is a hypervelocity launch system which uses a propulsive cycle similar to the one used in a ramjet engine. While the ram accelerator is structurally similar to a conventional gun, this combustion cycle creates a distinctly different pressure profile inside the barrel, and by extension a distinctly different stress and strain profile within the barrel itself. Finite Element Analysis (FEA) was performed using ABAQUS to investigate changes in barrel stress and strain due to transient loading conditions. The simulations showed maximum stress and strain decreasing with increasing projectile velocity, with maximum strain decreasing nearly 1.5 times more than the maximum stress despite remaining below the yield limit. Discontinuities in the inner surface of the barrel caused moderate increases to the maximum stress and strain. Testing also showed two specific velocities which created resonance responses within the system which amplified the stress and strain in the barrel.

TABLE OF CONTENTS

TABLE OF FIGURES iii

NOMENCLATURE iv

ACKNOWLEDGEMENTS v

Chapter 1 INTRODUCTION 1

Chapter 2 BACKGROUND 3

2.1 Ram Accelerator Operating Principles 3

2.2 Experimental Apparatus 4

2.2.1 Pre-launcher 4

2.2.2 Test Section 5

2.2.3 Decelerator Section 7

Chapter 3 Theory 8

3.1 Finite Element Analysis 8

3.2 Vibration 9

3.3 Pressure wave movement 12

3.3.1 Constant velocity 13

3.3.2 Constant acceleration 13

Chapter 4 METHODOLOGY 16

4.1 FEA model geometry 16

4.2 Mesh density and convergence testing 18

4.3 Material properties 20

4.4 Applied wave properties 20

4.5 ABAQUS DLOAD subroutine 20

4.6 Analysis cases 21

4.6.1 Control 21

4.6.2 Constant velocity 21

4.6.3 Contant acceleration 22

4.6.4 Frequency 23

Chapter 5 RESULTS AND DISCUSSION 24

5.1 Effect of Velocity 24

5.2 Effect of gaps in the tube 27

5.3 Resonance 32

5.3.1 Resonance mitigation 34

Chapter 6 CONCLUSION 35

6.1 Conclusion 35

6.2 Prospectus 35

BIBLIOGRAPHY 37

APPENDIX A 38

TABLE OF FIGURES

Figure 1.1: Pressure profiles: conventional gun vs. ram accelerator 2

Figure 2.1: Operational cycles: ram accelerator vs. ramjet 4

Figure 2.2: Experimental Apparatus 5

Figure 2.3: Ram accelerator internal profiles. 6

Figure 3.1: Vibration caused by moving pressure wave 10

Figure 3.2: Harmonics in the tube. 1st (top), 2nd (middle) and 3rd (bottom) harmonics .. 11

Figure 3.3: Frequency response 12

Figure 3.4: Resonance response over time 12

Figure 4.1: 3-D smooth-bore model 16

Figure 4.2: Axisymmetric smooth-bore model (axis of rotation shown in yellow) 16

Figure 4.3: 3-D baffle-tube model (mesh hidden for visibility) 17

Figure 4.4: Axisymmetric baffle-tube model 17

Figure 4.5: Non-applicable vibration (top) and applicable vibration (bottom) 23

Figure 5.1: Smooth-bore stress graph using constant velocity data 24

Figure 5.2: Smooth-bore strain graph using constant velocity data 25

Figure 5.3: Baffle-tube stress graph using constant velocity data 26

Figure 5.4: Baffle-tube strain using constant velocity data 26

Figure 5.5: Stress field at baffle gap 28

Figure 5.6: Strain lag in smooth-bore tube 29

Figure 5.7: Combined smooth-bore and baffle-tube strain 31

Figure 5.8: Smooth-bore combined constant v/a max stress 33

Figure 5.9: Smooth-bore combined constant v/a max strain 33

NOMENCLATURE

F	Force (N)
m	Mass (kg)
a	Acceleration (m/s^2)
ω	Frequency (Hz)
$G(\omega)$	Gain (as a function of frequency)
ω_n	Natural frequency (Hz)
v	Velocity (m/s)
λ	Wavelength (m)
t	Time (s)
x	Position (m)

Subscripts

0	Initial
f	Final

Abbreviations

UW	University of Washington
SBRA	Smooth-bore ram accelerator
RTRA	Rail-tube ram accelerator
BTRA	Baffle-tube ram accelerator
FEA	Finite Element Analysis
CFD	Computational Fluid Dynamics

ACKNOWLEDGEMENTS

I would like to thank Dr. Carl Knowlen for allowing me to work in the Ram Accelerator lab, and for guiding me through the process of researching and writing my thesis. Thanks as well to Dr. Brian Leege for serving on my thesis committee and providing insightful commentary on my work.

I would also like to thank all my friends and family who have supported me throughout my studies, I wouldn't be where I am, or who I am today without all of you.

Chapter 1

INTRODUCTION

Ram accelerator is a hypervelocity launch system which is theoretically capable of firing a capsule from the surface of Earth into orbit with minimal usage of onboard propulsion. This technology was first developed at the University of Washington (UW) in the 1980s, since then researchers at the UW have continued to improve the ram accelerator, leading to projectile velocities of 2.7 km/s, with a theoretical maximum velocity of 12 km/s. [1]

One of the primary drivers for the development of ram accelerator is its potential as a space launch system. Currently, the only way of getting payloads into space is using rockets, which have the distinct disadvantage of having to carry their fuel with them. Rockets typically can only carry a small fraction of their total mass as payload, which is why it currently costs $2720/kg to launch material into low Earth orbit [2] . As mentioned above, the fuel in the ram accelerator is in the barrel rather than the projectile, this means a space capsule fired via ram accelerator can carry a very high percentage of its mass as payload, which significantly reduces launch costs.

The ram accelerator shares many similarities with a conventional gun, as both use combustion to fire projectiles through long barrels. However, one key difference is that a bullet from a conventional gun is propelled by the expansion of pressurized combustion products from a breech, whereas a ram accelerator projectile is propelled by a continuous combustion process which follows the projectile. This leads to a very different pressure profile within the barrel while the projectile is being fired as can be seen in Figure 1.1. In a conventional gun, the pressure is at

its highest immediately after firing and as the bullet travels down the barrel, the combustion gasses expand to fill the space, which lowers the pressure. In a ram accelerator the continuous combustion process creates a high-pressure region that travels with the projectile down the barrel.

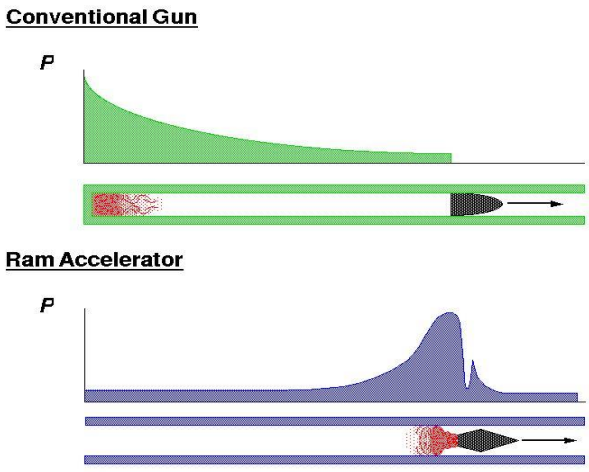

Figure 1.1: Pressure profiles: conventional gun vs. ram accelerator

While the response of a conventional gun barrel to the pressure of firing is well documented, the response of a barrel to the pressure of a firing ram accelerator are largely unknown, and it is this response that is the focus of this investigation. Specifically, this paper focused on answering three questions.

1. How does projectile velocity effect the stress and strain response of the barrel?
2. How will gaps in the inner surface of the barrel (like those introduced by non-gastight baffles) effect the stress and strain response of the barrel?
3. Will the vibrations induced by the projectile as it is fired create a resonance response in the barrel, and if so, what is the nature and location of this response?

Chapter 2

BACKGROUND

2.1 Ram Accelerator Operating Principles

The ram accelerator works on similar principles to a ramjet engine. Figure 2.1 shows the ramjet engine cycle; in it, air that is travelling at supersonic speeds relative to the engine is diffused by the area contraction of the centerbody and is brought to subsonic velocity by the normal shock that is stabilized behind the throat of the diffuser. Fuel injection and combustion occur sub-sonically within the engine and the flow is then accelerated out the back of the engine through a converging-diverging nozzle. The ram accelerator alters this process by replacing the centerbody, which is connected to the ramjet engine cowling, with a similarly shaped projectile. Because this projectile is not connected to the rest of the engine, the thrust generated by the combustion process propels the projectile forward within the tube. Additionally, the incoming air is replaced with a fuel/oxidizer mixture, which means the projectile does not need to carry its own fuel, as a ramjet or rocket would.

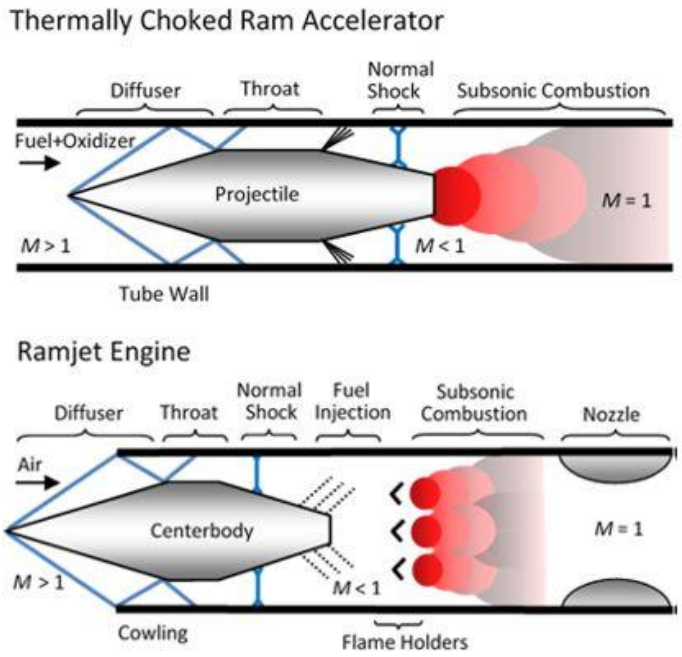

Figure 2.1: Operational cycles: ram accelerator vs. ramjet

2.2 Experimental Apparatus

A diagram of the UW ram accelerator system can be seen in Figure 2.2, the system can be separated into three sections, the pre-launcher, the test section, and the deceleration section.

2.2.1 Pre-launcher

The ram accelerator cannot operate with a projectile below a certain velocity, so another method is needed to accelerate it up to around 1 km/s before the test section. One option for this task is a light gas gun as can be seen in Figure 2.2, which operates by bursting a diaphragm that separates a pressurized helium reservoir from the 38-mm-bore launch tubes (which are evacuated of gasses before firing) where the projectile is loaded. The pressure of the expanding helium pushes the projectile up to speeds that allow the ram accelerator to function. Other potential candidates for

the pre-launcher stage include conventional solid propellant guns, combustible gas guns, and electromagnetic launchers (i.e. coilguns and railguns).

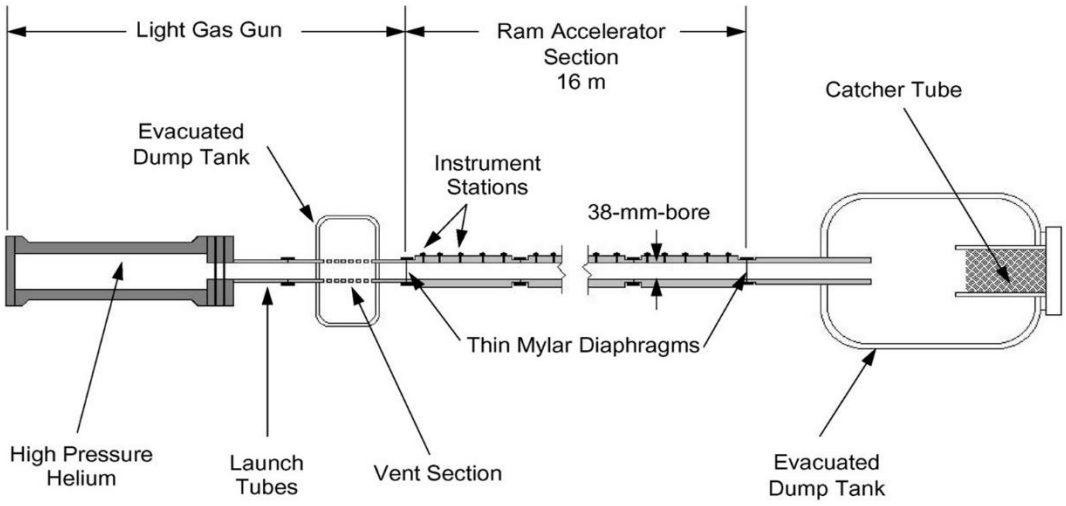

Figure 2.2: Experimental Apparatus

2.2.2 Test Section

The central portion of the system is the test section, which was the focus of the analysis done in this paper. The ram accelerator section consists of a series of tube segments, attached together to create a continuous barrel. The tube segments can be separated by Mylar diaphragms which allows for stages of differing gas composition and pressure within a single test. Staging in this manner allows for the manipulation of gas properties across the length of the ram accelerator. This is important because a given gas mixture is only able to operate efficiently over a limited velocity range. This becomes even more important when looking at space launch applications that could see velocities ranging from 6-8 km/s [3], requiring multiple different gas mixtures to operate

efficiently. Figures 2.2 and 2.3 show instrument stations that allow for the collection of data during a shot. Data from these instruments are used in this investigation, the stations themselves were not added to the barrel simulations as they are experimental tools and would not be present in practical application.

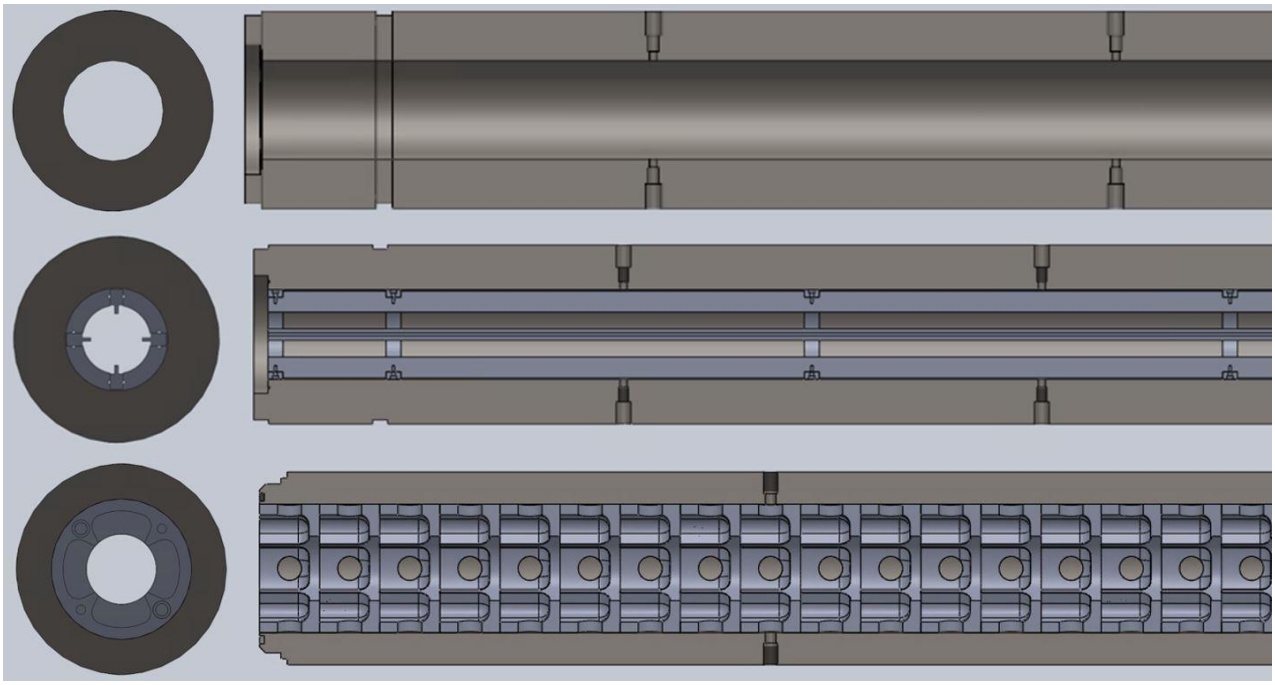

Figure 2.3: Ram accelerator internal profiles.

Top: SBRA Middle: RTRA Bottom: BTRA

Figure 2.3 shows the three different internal structures for ram accelerator tubes, smooth-bore, rail-tube, and baffle-tube. As the name suggests, the smooth-bore ram accelerator (SBRA) features a smooth circular bore. This was the first configuration developed and is the simplest of the three. The rail tube ram accelerator (RTRA) uses a similar tube to the smooth-bore configuration, but it adds rails which are equally spaced around the inner surface of the tube. These rails run the length of the tube and support the projectile in flight, preventing it from canting within

the tube. The baffle tube ram accelerator (BTRA) also uses inserts to modify the internal geometry of the tube, and the inserts serve to stabilize the projectile within the tube, much like the rails in the RTRA. More information about the geometry of the baffle inserts and the overall configuration of the BTRA can be found in [4].

2.2.3 Decelerator Section

For testing purposes, the system needs to not only accelerate the projectile, but also decelerate and contain the projectile and the exhaust gasses from the ram accelerator process. In the system depicted in Figure 2.2, the dump tank is used to collect the hot exhaust gasses from the ram accelerator. On the back wall of the dump tank is the catcher tube, which is packed with material that decelerates the projectile to mitigate the impact on the wall of the tank. The decelerator section is obviously not needed in real-world applications where the goal is to exit the barrel at high velocity.

Chapter 3

Theory

3.1 Finite Element Analysis

Most structural engineering problems are governed by differential equations, the most common example being Newton's Second Law $F=ma$ which governs all dynamics problems (it governs statics problems as well, but since the acceleration term is zero, the resulting equation is not generally a differential equation.) For Newton's Second Law, if the force in the problem varies with position (which will almost always be the case), the equation becomes a second order ordinary differential equation. This is a simple example of a governing differential equation, however when considering problems with complex geometry and loading conditions, these differential equations can quickly become nearly unsolvable in closed form. Complex differential equations often require a great deal of manipulation to solve, which can be very unintuitive. The leaps of logic required for this type of solving are very difficult for a computer to perform.

This is where Finite Element Analysis (FEA) excels, as it converts complex differential equations into many simple linear equations. While this process exponentially increases the number of equations to be solved, the simpler nature of the equations allows FEA to solve problems far more efficiently. To accomplish this conversion of equations, FEA divides the body up into a number of finitely sized elements with nodes at each corner (and sometimes additional nodes along the edges). The system of linear equations is then solved, which gives exact values at each node, but requires interpolation to get any value between the nodes. This answer is an estimate of the closed-form solution (with the exception of some very simple systems where the interpolation between nodes gives the exact solution), but as element size approaches zero it

converges to the closed form solution. Importantly, however, as the element size approaches zero, the number of elements approaches infinity, so the number of elements chosen for a given problem is a tradeoff between accuracy and the computational intensity of the system. To determine the correct element size for a given problem, convergence testing is used. Convergence testing is performed by running a series of simulations with steadily decreasing element size and looking at the percentage change in the output variable of interest. Once the change between consecutive simulations is below an acceptable threshold, the FEA analyst can use that element size to simulate the system without fear of excessive error due to element size.

3.2 Vibration

As the projectile moves through the ram accelerator, the combustion process that creates thrust also creates a band of very high pressure which travels with the projectile. As this band of pressure passes over an area, stress is applied to the inner wall of the tube. This stress creates distortion which can be seen as the tube bulging slightly. This outward distortion and the subsequent springing back after the projectile has passed creates a vibrational wave within the tube that can be seen in Figure 3.1.

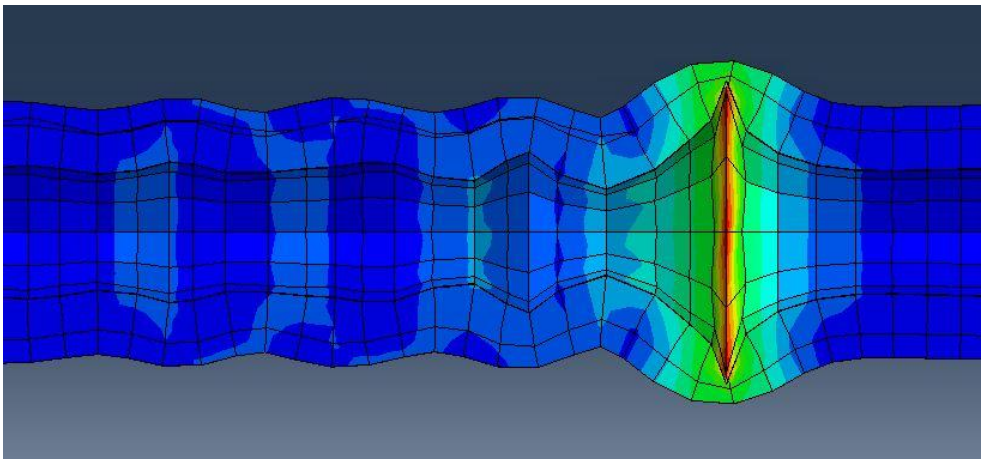

Figure 3.1: Vibration caused by moving pressure wave

The response a given structure will have to an applied vibration is affected by both its material properties and the geometry of the part, which together create its natural frequency, the frequency at which it will vibrate continuously (for a case with no damping) in response to an initial displacement, and no other externally applied forces. More complex geometries can have multiple natural frequencies corresponding to different modes of vibration. Some of these additional natural frequencies will be integer multiples of an earlier one, these are known as harmonics and they represent the same vibrational shape but with additional nodes. Figure 3.2 shows the first three harmonics of the vibrational shape of interest for this analysis.

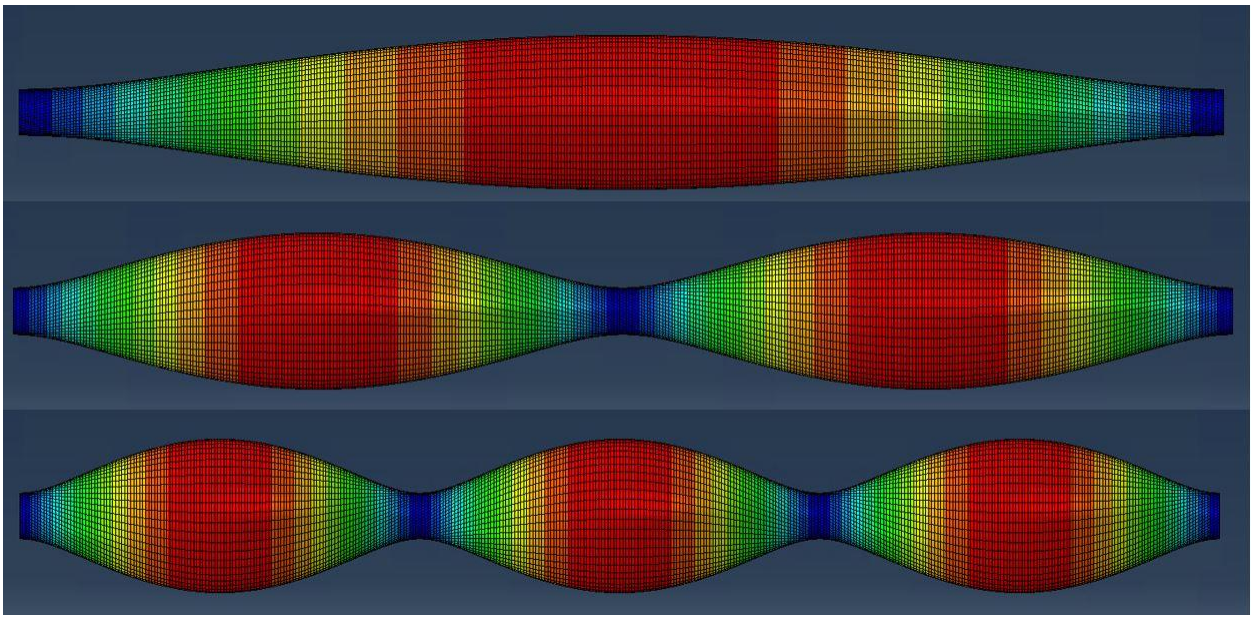

Figure 3.2: Harmonics in the tube. 1st (top), 2nd (middle) and 3rd (bottom) harmonics

The natural frequency is very important in vibrational analysis because if an externally applied vibration is very close in frequency to one of the system's natural frequencies it can lead to a state of resonance which can in turn lead to excessive stresses and strains in the system.

Figure 3.3 shows how the gain ($G(\omega)$) or amplification of the system changes with frequency (ω), when the frequency approaches the natural frequency (ω_n), the gain reaches its maximum value; this response is called resonance. The longer the system stays in a state of resonance, the more the response to the applied vibration will grow which is shown in Figure 3.4. The amount of amplification experienced in a resonance state is dependent on which natural frequency is being approached, and how the vibration is applied to the system. For the ram accelerator, operating in a sufficiently strong resonance state for an extended period of time could lead to unexpectedly high stress and deformation in the tube wall or even catastrophic failure of the tube itself.

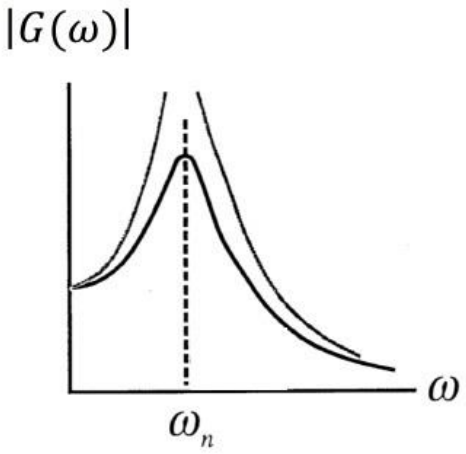

Figure 3.3: Frequency response

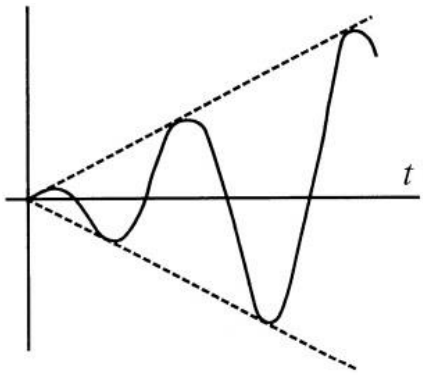

Figure 3.4: Resonance response over time

Because the ram projectile is accelerating, the velocity of the projectile will be constantly changing, as will the pressure wave that drives it and applies the load to the tube. The frequency (ω) of the vibration being applied by the pressure wave is a function of that velocity (v) and the wavelength (λ), according to Equation 3.1.

$$\omega = \frac{v}{\lambda} \tag{3.1}$$

Because the projectile traverses such a wide range of velocities in the ram accelerator, the chance of crossing through a region where the generated waveform's frequency is equal to a natural frequency of the tube is greatly increased. This is why it is important to understand where resonance occurs and how to mitigate it.

3.3 Pressure wave movement

In order to simulate the movement of the pressure wave in the FEA simulations, equations needed to be developed to calculate the position of the wave's center based on the elapsed time. For the

stationary control tests, the wave center was set to a constant 1 m, corresponding to the center of the 2-m-long tube.

3.3.1 Constant velocity

For the constant velocity case, start by defining velocity as some constant value *v* (Equation 3.2), then integrating once with respect to time to get Equation 3.3 (by evaluating the integrals at $t = 0$ the constant of integration can be found to be initial position x_0).

$$v = \frac{dx}{dt} \tag{3.2}$$

$$x = v * t + x_0 \tag{3.3}$$

All simulations were performed such that the pressure wave started exactly at one end of the tube and finished exactly at the other end, which means that the initial position $x_0 = 0$. It also means a different time period is needed for each simulation with a different velocity. The time period can be easily found by solving Equation 3.3 for *t* using the end of the tube as a boundary condition to find the final time (t_f) (because the system starts at $t = 0$ the final time is equal to the time period).

$$t_f = \frac{x_f}{v} \tag{3.4}$$

3.3.2 Constant acceleration

For the constant acceleration case, start by defining acceleration as some constant value *a* (Equation 3.5), then integrating twice with respect to time as follows (by evaluating the integrals at $t = 0$ the constants of integration can be found to be initial velocity v_0 and initial position x_0 respectively).

$$a = \frac{dv}{dt} \tag{3.5}$$

$$v = at + v_0 \tag{3.6}$$

$$x = \frac{1}{2}at^2 + v_0 t + x_0 \tag{3.7}$$

The required values for the constant acceleration tests can be found in a similar way to the constant velocity case, though the process is made more complicated because the boundaries imposed for the test are not in terms of a and v_0, instead they are in terms of v_0 and v_f. To find the appropriate values for a, v_0, and t_f, start with the definition of a constant acceleration as change in velocity over change in time. For all the cases used in this analysis $t_0 = 0$, so this term is removed for all further calculations.

$$a = \frac{v_f - v_0}{t_f - t_0} \tag{3.8}$$

This equation along with Equations 3.6 and 3.7 form the system of equations which can be used to solve for a, v_0, and t_f. First, Equation 3.6 is solved for v_0 and substituted into Equation 3.7. Additionally, as was mentioned above, the pressure wave will always begin the test at the beginning of the tube so $x_0 = 0$.

$$x = -\frac{1}{2}at^2 + vt \tag{3.9}$$

Because this is a quadratic equation, the quadratic formula can be used to solve for t resulting in Equation 3.11.

$$t = \frac{-(-v) \pm \sqrt{(-v)^2 - 4\left(\frac{1}{2}a\right)(x)}}{2\left(\frac{1}{2}a\right)} \tag{3.10}$$

$$t = \frac{v \pm \sqrt{v^2 - 2ax}}{a} \tag{3.11}$$

Equation 3.11 produces 2 answers due to the ± criteria. Examining Equation 3.11 shows that for this case, where *v*, *a*, and *x* are all positive real numbers, the positive branch of the ± has t increasing with decreasing values of x. This would imply backwards movement which is impossible when velocity, acceleration and position are always positive, therefore only the negative branch is a valid solution. Equation 3.11 is evaluated at $t = t_f$ and then substituted into Equation 2.8 and solved for *a*.

$$a = \frac{{v_f}^2 - {v_0}^2}{2x_f} \tag{3.12}$$

The value v_f is a parameter chosen for a given simulation, and x_f is equal to the length of the test section. By substituting in the appropriate values for the case being run, Equation 3.10 can be solved for *a*. This value can be plugged into Equation 3.11 and evaluated at $t = t_f$ to solve for t_f. Finally, plug *a*, t_f, and v_f into Equation 3.4 to solve for v_0, which is the last value needed to characterize the movement of the pressure wave.

Chapter 4

METHODOLOGY

4.1 FEA model geometry

All modelling for this study was done in Abaqus 2022 using the standard solver. All values used were in base metric units (m, kg, and s). Early in this study, both 3D and axisymmetric models were created (Figures 4.1 and 4.2) and for a given set of inputs, both showed similar results. However, it was immediately apparent that the axisymmetric model was superior to the 3D for nearly all cases, as the axisymmetric model was able to complete simulations with element sizes that were 8-10 times smaller than the 3D model in similar amounts of time.

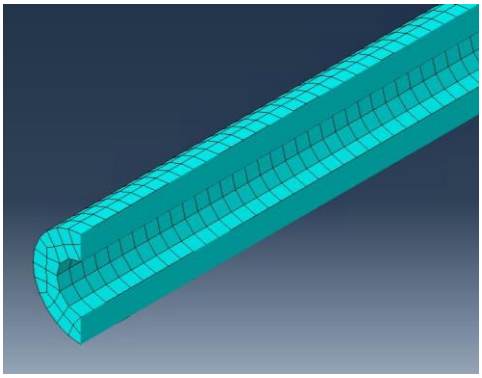

Figure 4.1: 3-D smooth-bore model

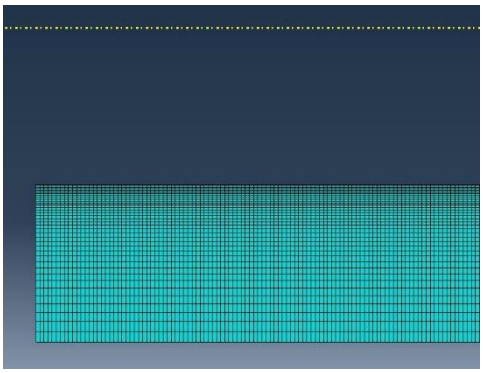

Figure 4.2: Axisymmetric smooth-bore model (axis of rotation shown in yellow)

The smooth-bore model consisted of a 2-m-length of 38.1 mm (1.5 in.) bore, 19.1 mm (0.75 in.) thick tube as can be seen in Figures 4.1 and 4.2. The ends of the tube are held fixed, the

localized error introduced by this boundary condition was mitigated by taking measurements at or near the middle of the tube.

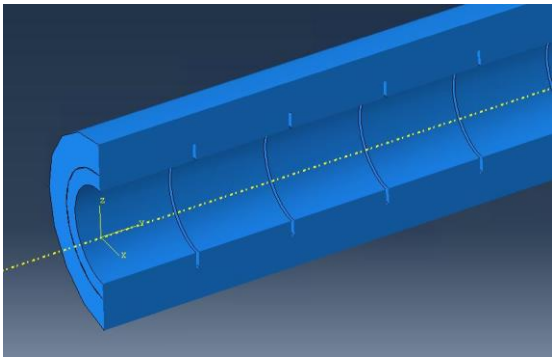

Figure 4.3: 3-D baffle-tube model (mesh hidden for visibility)

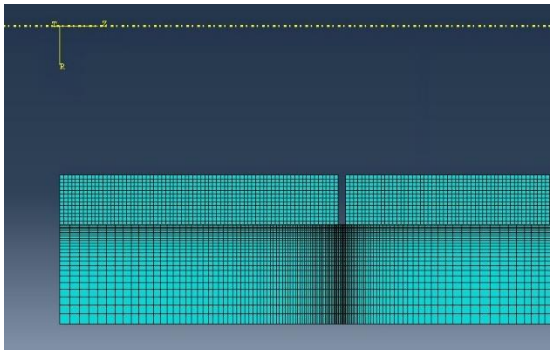

Figure 4.4: Axisymmetric baffle-tube model

The baffle-tube model introduced added complexity over the smooth-bore model. The shell tube has the same outer diameter as the smooth-bore tube, but it is only 12.7 mm (0.5 in.) thick. This shell tube is lined with a series of simplified baffles as seen in Figures 4.3 and 4.4. These simplified baffles are short sections of tube whose outer surface is flush with the inner surface of the shell tube and are 6.35 mm (0.25 in.) thick, resulting in the same equivalent thickness as in the smooth-bore tube. The simplified design of the baffles allows them to be used in axisymmetric modeling, as well as easier study of the thinnest section of the baffles without the stiffening effect of the main baffle plate. The baffles are placed with a 1 mm gap between them. This gap is far larger than what would appear in a real system, but it allowed for the investigation into the effects of gas leaking through the interface between baffles and imparting pressure directly onto the wall of the shell tube. If high levels of stress and strain were discovered in the shell tube wall due to the directly applied pressure, more tests could be run with narrower baffle-gaps to better simulate a more realistic scenario. The baffles were allowed to slide frictionlessly along the

length of the shell tube, apart from the stationary control case that is discussed later. This condition seemed to have little effect however, since the radial pressure wave did not induce noticeable translations in any of the moving-wave cases. The outer surfaces of the baffles were forced to stay in contact with the shell tube, because early simulations showed that allowing these surfaces to separate induced so much instability in the system that solutions could not be reached in a reasonable time.

4.2 Mesh density and convergence testing

The first simulations run after the model geometry was finalized were the convergence tests. Convergence tests were run for both the smooth-bore and the baffle-tube configurations, starting with a 4 mm element size, and reducing by half with each successive step until the percentage change in maximum stress and strain between tests was below 1%. All convergence testing was performed on the 1000 m/s constant velocity simulation. Time step convergence testing is handled internally by ABAQUS.

The mesh for all configurations used CAX8R elements which are 8-node quadrilateral elements, having one node at each corner and one at the center of each edge. This element type showed better convergence results than the default 4-node quadrilateral.

The mesh of the smooth-bore model, which can be seen in Figure 4.2, began with an evenly spaced rectangular mesh, and then a bias was added to the radial direction, which means that the elements near the inner surface of the tube are much smaller, and they gradually increase in size as they move to the outside surface.

The mesh of the baffle-tube model, which can be seen in Figure 4.4, began with the same rectangular mesh with a bias toward the inner surface as the smooth-bore test. The addition of the

baffles and gaps between them necessitated more manipulation of the mesh. A bias was added along the length of the shell tube underneath each baffle, decreasing the mesh size near the gaps and increasing it in the middle of the baffles. The baffles themselves used a simple rectangular mesh because their position on the inside of the tube and their relative thinness meant they were likely to see high concentrations of stress/strain throughout, which would make biasing toward any one direction inadvisable.

Table 4.1 shows convergence testing results for both smooth-bore and baffle-tube configurations (tested at the middle of a baffle and at a gap between baffles). For all configurations, a global element size of 0.5 mm was sufficient to reduce the percentage change between successive tests to below the 1% threshold.

	Smooth-bore		Baffle (Mid-baffle)		Baffle (Gap)	
Element size (mm)	Δ% Stress	Δ% Strain	Δ% Stress	Δ% Strain	Δ% Stress	Δ% Strain
4	N/A	N/A	N/A	N/A	N/A	N/A
2	0.70%	3.27%	0.73%	2.31%	5.82%	6.84%
1	1.70%	0.07%	0.67%	0.42%	0.56%	1.56%
0.5	0.05%	0.00%	0.57%	0.83%	0.78%	0.99%

Table 4.1: Convergence test results

4.3 Material properties

The material used in all tests is AISI 1060 carbon steel. The material properties of interest to this project are a density of 7850 kg/m^3, a modulus of elasticity of 205 GPa, a Poisson's ratio of .29, a yield strength of 485 MPa, and an ultimate strength of 814 MPa. [5] The first three of these properties (density, modulus of elasticity, and Poisson's ratio) were simulation parameters, and their values can be regarded as representative of any carbon steel. This means that simulating the system with any grade of carbon steel would give similar results to those presented here.

4.4 Applied wave properties

Previous ram accelerator CFD studies [6] and ram accelerator experimental data [7] show a very complex pressure field around the projectile. For the purposes of this study, a 10 mm wide square wave corresponding to a 10 μs pulse at 1 km/s was used to simulate the primary pressure spike that travels with the projectile. This simplification neglects the region of pressure that follows the initial spike, more complex pressure profiles that better simulate this region represent an avenue of future research. Likewise, the experimental results presented in [6] shows the pressure ratio in the barrel depends on Mach number, this relationship was simplified to a constant pressure of 344 MPa (50 ksi) to represent a wide range of projectile velocities.

4.5 ABAQUS DLOAD subroutine

Because of the complexity of the loading condition, the Abaqus user-defined function DLOAD was required. This is a Fortran code file which is attached to every simulation which defines the loading parameters for the test. The code written for this project operated by taking a time input from the system and using that to calculate the location of the center of the pressure wave as

discussed in Chapter 3. It then instructed Abaqus to apply a 345 MPa (50 ksi) pressure to any nodes that were no more than half the width of the wave (5 mm) away, and to apply zero pressure to any nodes outside that band. A sample DLOAD file can be found in Appendix A.

4.6 Analysis cases

The cases run can be broken down into four categories: control, constant velocity, constant acceleration, and frequency response. Each of these cases was run in both the smooth-bore and baffle-tube configurations.

4.6.1 Control

The control case for the smooth-bore had the applied pressure wave sitting stationary at the center of the tube, and was run for a duration of one second to allow transient effects to disappear. Two control cases were run for the baffle-tube with the same setup as the smooth bore apart from the location. The baffle-tube control simulations were run over the full length of the tube with the pressure wave first centered on a baffle, and second centered on a gap between the baffles (both simulations were run near the center of the tube.) These tests were intended to find the steady-state response to the applied pressure wave.

4.6.2 Constant velocity

For the constant velocity cases, the applied pressure wave began at one end of the tube and moved toward the other end at the specified velocity. The duration of the simulation was chosen such that the simulation finished when the wave reached the end of the tube. Constant velocity tests were run for velocities between 1 km/s and 6 km/s at 0.5 km/s intervals (extra tests were done after the

main series to resolve resonance points.) These tests were intended to collect data on how the barrel response changed with wave velocity, to compare data between the smooth-bore and baffle-tube cases to find the impact of the baffle gaps, and to look for peaks in stress and strain that could indicate resonance conditions.

4.6.3 Contant acceleration

The constant acceleration simulations followed the procedure for the constant velocity simulations, except that instead of having many cases run between the minimum and maximum velocities, the wave would move between the minimum and maximum velocities as it moved down the length of the tube. To avoid the error induced by the boundary conditions, the constant acceleration cases began with an initial velocity of 0 km/s. A similar adjustment was not needed at the other end, because the vibrational waves in the simulation did not propagate ahead of the applied pressure, which mitigates the effects of the boundary condition at the end. These simulations were intended as another way to look for resonant conditions.

4.6.4 Frequency

The frequency simulations are the only cases that do not use the applied pressure wave, instead ABAQUS applies a specified range of frequencies to the model to find the natural frequencies. This means that this simulation finds natural frequencies for non-applicable vibrational modes, so the data needs to be analyzed to isolate only the dominant natural frequencies (Figure 3.5).

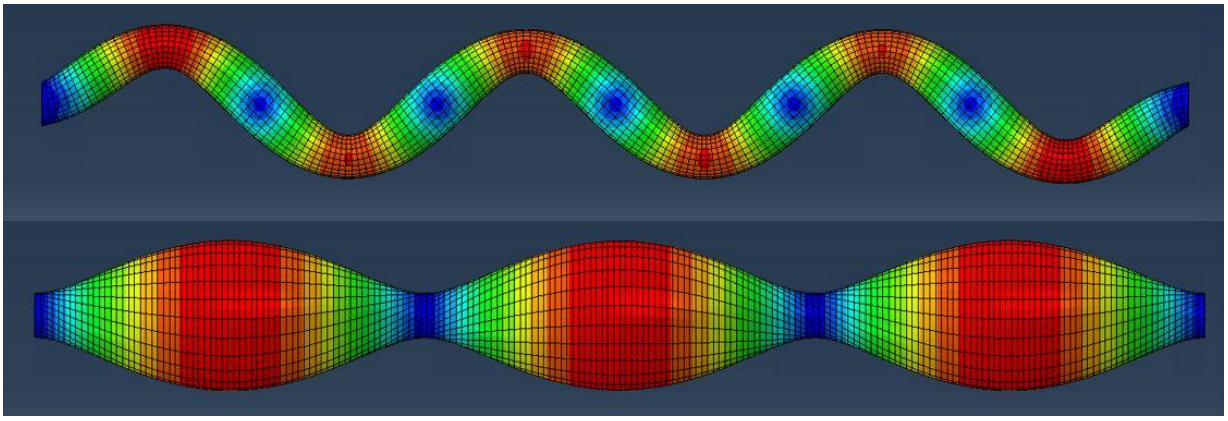

Figure 4.5: Non-applicable vibration (top) and applicable vibration (bottom)

The frequency tests were done using a 3D model instead of the axisymmetric model because the mode shapes were more complicated to analyze when using the axisymmetric model. This test found natural frequencies for all harmonics of a given vibrational mode within the specified frequency range, though only the fundamental frequency was needed as the frequencies for all higher harmonics were integer multiples of the fundamental frequency. By measuring the wavelength in a constant velocity test, the frequency applied by the pressure wave can be found using Equation 2.1 and compared against the natural frequencies.

Chapter 5

RESULTS AND DISCUSSION

5.1 Effect of Velocity

Examining the constant velocity simulation results for the smooth-bore configuration, a clear trend of decreasing maximum stress and strain with increasing velocity can be seen. In both Figures 5.1 and 5.2, two prominent local maxima are visible, these are resonance points and they will be discussed in detail in section 5.3. Unless otherwise noted, all stress measurements are maximum von Mises stresses, all strains are maximum principal strains, and the horizontal red lines indicate yield stress/strain.

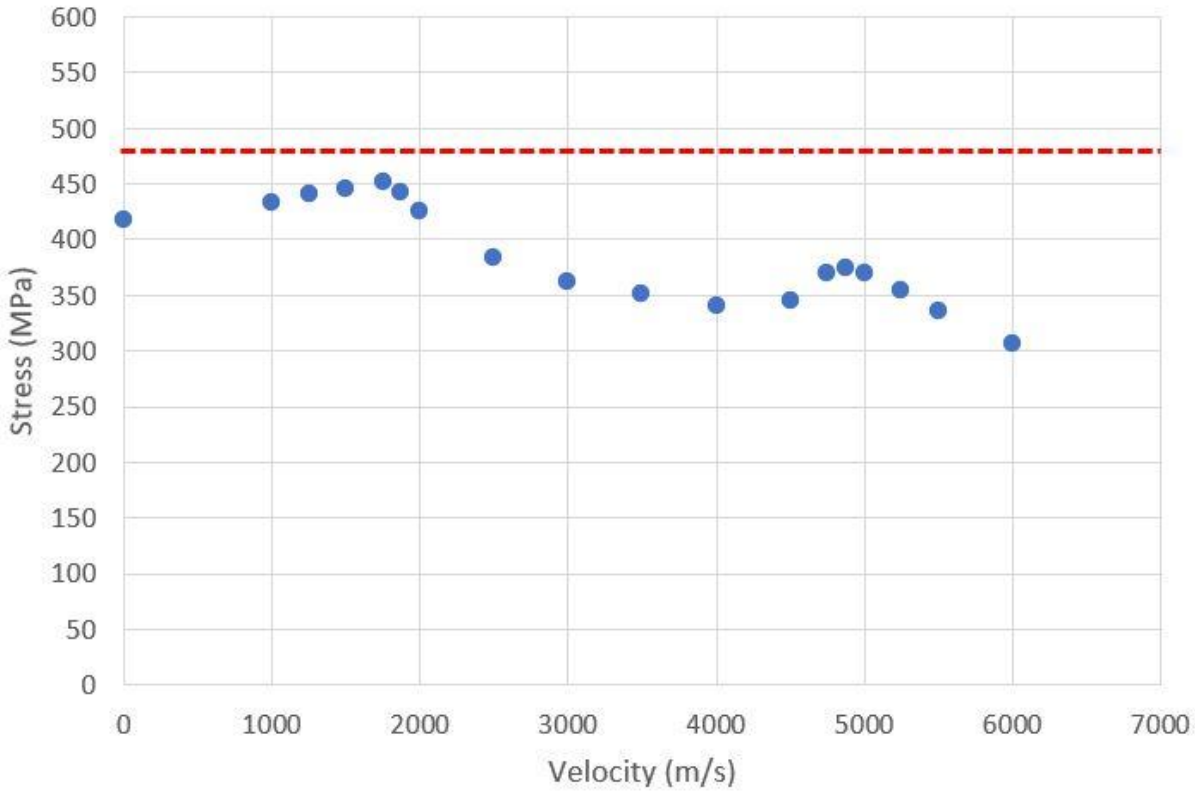

Figure 5.1: Smooth-bore stress graph using constant velocity data

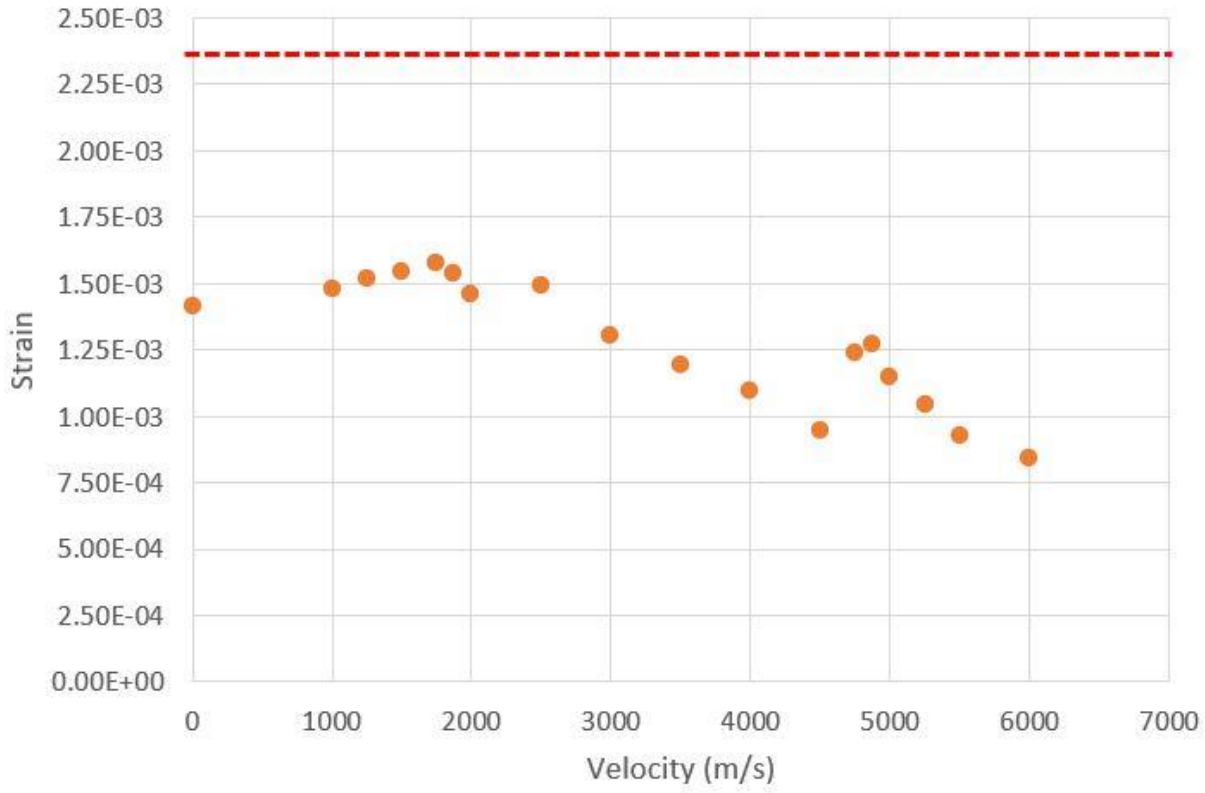

Figure 5.2: Smooth-bore strain graph using constant velocity data

Figures 5.3 and 5.4 show the stress and strain responses for the baffle-tube configuration. Both the stress and strain plots show three sets of results corresponding to when the pressure wave was centered on a baffle, and when the pressure wave was centered on a gap between baffles, with an extra case where the pressure wave was centered on the gap but the measurements were taken from the inner surface of the shell tube. The significance of these three separate measurements is discussed in section 5.2. All three sets of results exhibit the same general trend as the smooth-bore figures with decreasing stress and strain for increasing velocity.

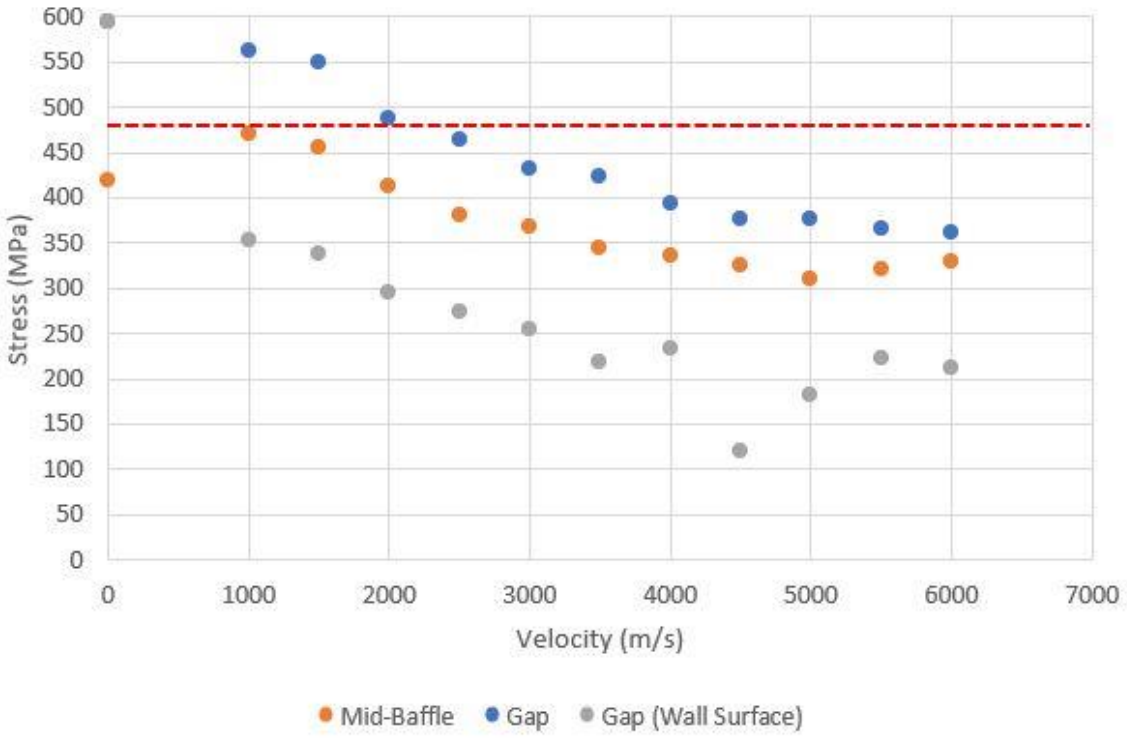

Figure 5.3: Baffle-tube stress graph using constant velocity data

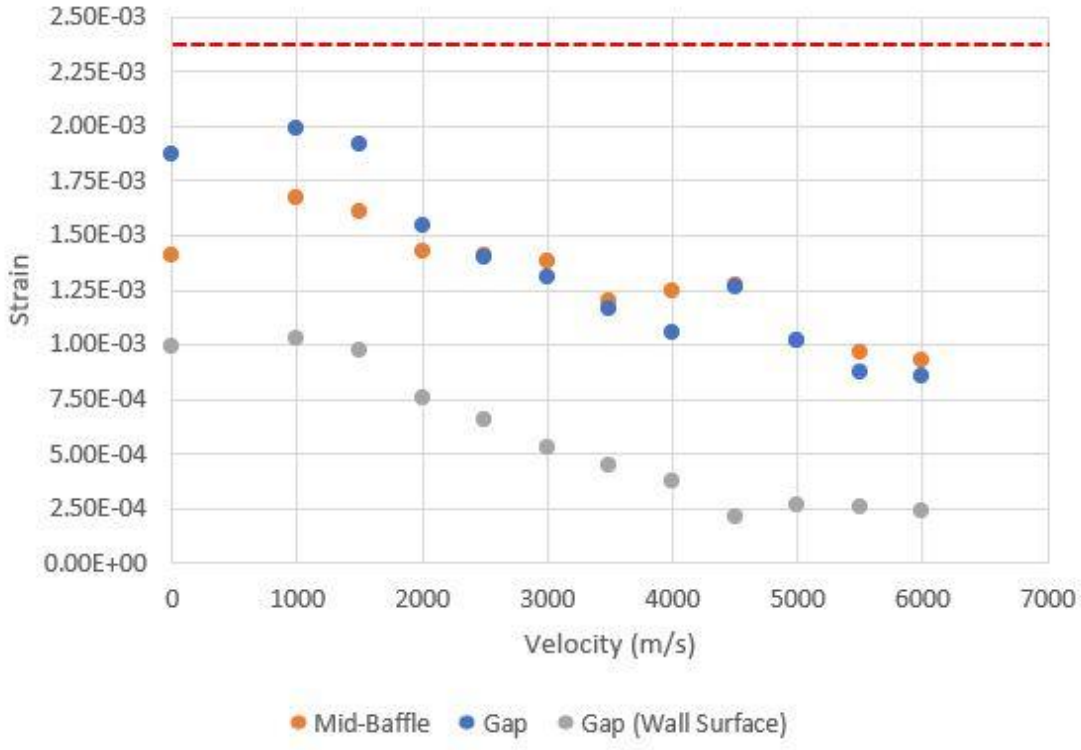

Figure 5.4: Baffle-tube strain using constant velocity data

As velocity increases, the time any given point in the tube has pressure applied to it decreases. As can be seen in Figures 5.1-5.4 this reduction in duration of applied pressure leads to reduced maximum stress and strain. The maximum stress and strain do not, however, decrease at the same rate despite being below the yield limit where a linear stress-strain relationship would be expected; between 1000 m/s and 6000 m/s in the smooth-bore configuration the maximum stress fell by 29%, while the maximum strain fell by 43%. This result is significant because all results for both configurations showed strain below the yield strain of the material, meaning the tube is in the region of elastic deformation where the stress and strain should exhibit a linear relationship (stress and strain decreasing at an equal rate). This suggests that for higher velocities, maximum stresses above the material's yield stress may correlate to maximum strains below the yield strain limit, meaning it may be possible to exceed the material's yield strength without damaging the material.

5.2 Effect of gaps in the tube

Figure 5.3 shows that for all velocities in the baffle tube configuration, the highest stresses were found when the pressure wave passed the gap, and for all these cases the highest stresses were found at the tips of the baffles as seen in Figure 5.5. (The one exception is the control case, though this is likely due to removing the baffles' ability to slide along the tube.) The next highest stresses occurred in the mid-baffle cases, with the gap wall surface showing the lowest stresses across all velocities (again excluding the control).

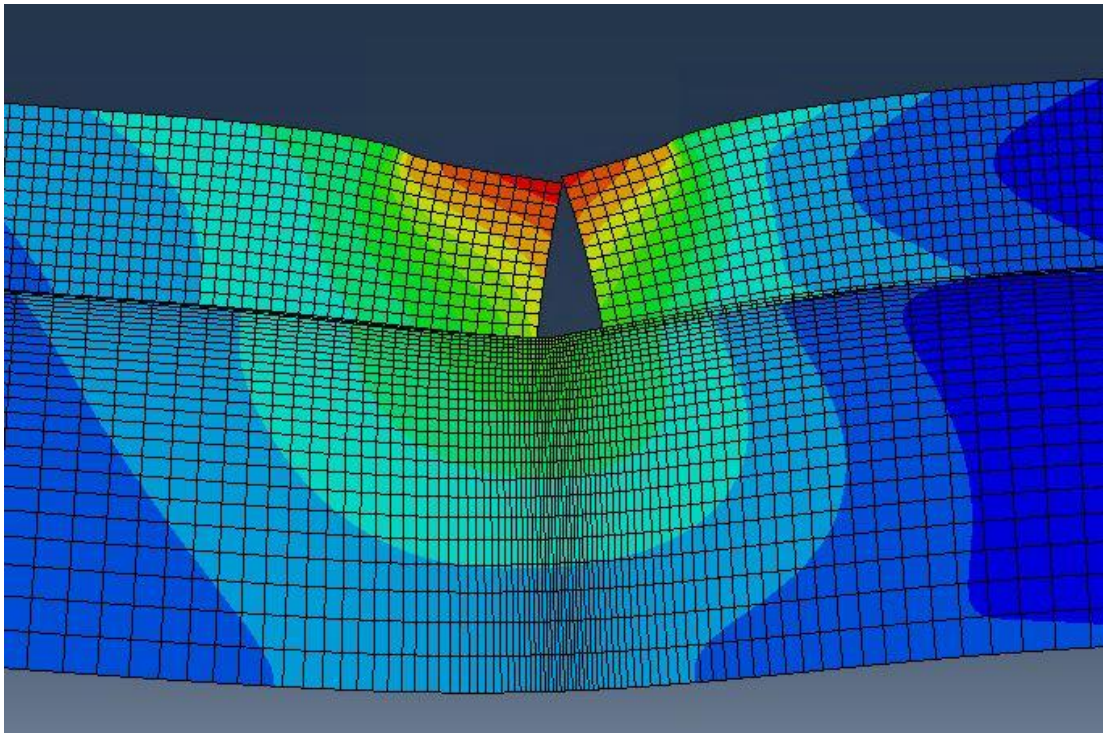

Figure 5.5: Stress field at baffle gap

Deformation scaled up 100x for visibility, red areas denote maximum stress

The strain curve in Figure 5.4 shows a similar general shape to the stress curve, with the notable exception that the mid-baffle strain overtakes the gap strain for velocities above 2000 m/s. This phenomenon occurs because the data was taken when the pressure wave, and the corresponding maximum stress area were at the prescribed points (either mid-baffle or baffle gap). As the velocity increased, however, a time lag developed between the location of the maximum stress and the location of the maximum strain as can be seen in Figure 5.6, which shows this effect in the smooth-bore configuration.

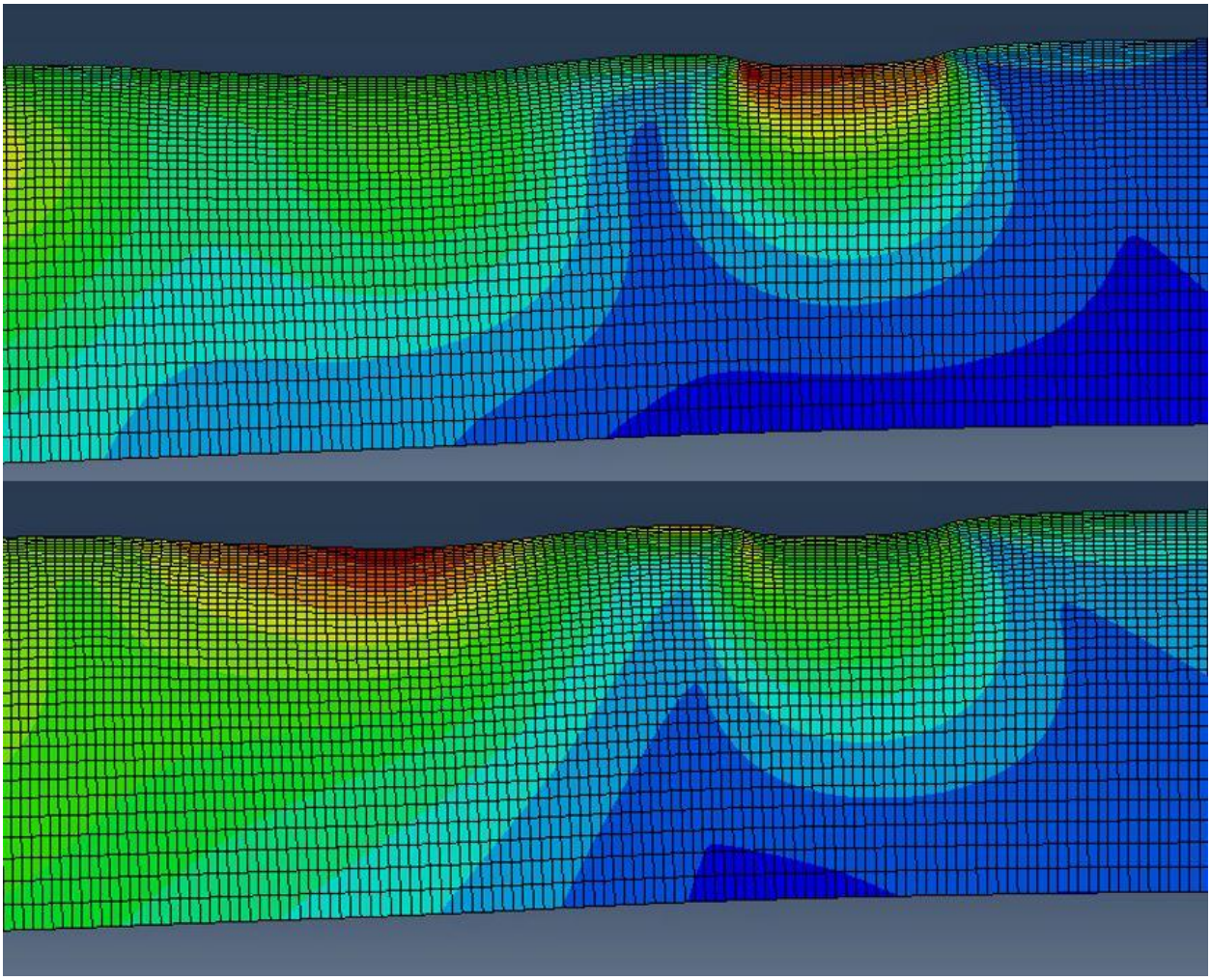

Figure 5.6: Strain lag in smooth-bore tube

Stress field (top) and strain field (bottom) for same time and location from 4500 m/s test

The smooth-bore configuration allows for this strain lag phenomenon to be more easily seen and understood due to its uniform geometry; however, this geometric consistency also means that the strain lag has less effect. The baffle-tube configuration exhibits the same strain lag, but due to the inconsistent geometry caused by the gaps between the baffles the impact on the simulation results is much larger. As noted earlier, the strain values for the mid-baffle and gap seen in Figure 5.4 seem to cross over each other around the 2500 m/s mark. This is because at this

speed the strain lag has reached a point where the maximum stress is at the mid-baffle point corresponds to a maximum strain that has moved back to the gap and vice versa.

Because both the smooth-bore and baffle-tube configurations had the same bore size and effective wall thickness, the results of the two tests can be directly compared to determine the impact of the gaps on stress and strain response of the tube. Results from velocities with both smooth-bore and baffle-tube simulations indicate that the addition of the 1 mm gaps into the baffle-tube model led to an average 16.68% increase in stress, and a 13.44% increase in strain. By only considering where both configurations had constant velocity results, the additional cases from the smooth-bore simulations around the resonance points were excluded, reducing the confounding effect of resonance on these results.

One of the primary reasons for simulating the baffle-tube configuration was to assess the risk posed by using baffles that did not form a gas-tight seal. While in this model pressure is applied directly to the inner surfaces of the components, in the real ram accelerator that pressure is applied through expanding gasses, and because the individual baffles do not form a gas-tight seal with each other some amount of gas will pass through the gaps and apply pressure to the shell-tube wall directly.

Despite using gaps far larger than any that would appear in a real ram accelerator, Figure 5.7 shows that the maximum strains at the wall of the shell tube are consistently lower than the maximum values for any of the other locations, including the smooth-bore (stress data omitted for brevity as it follows the same trends as the strain data.) This suggests that while the leakage between baffles will increase stress and strain in the shell-tube, it is unlikely that when considering more realistic baffle gap widths that it will create serious stress or strain concentrations at those points.

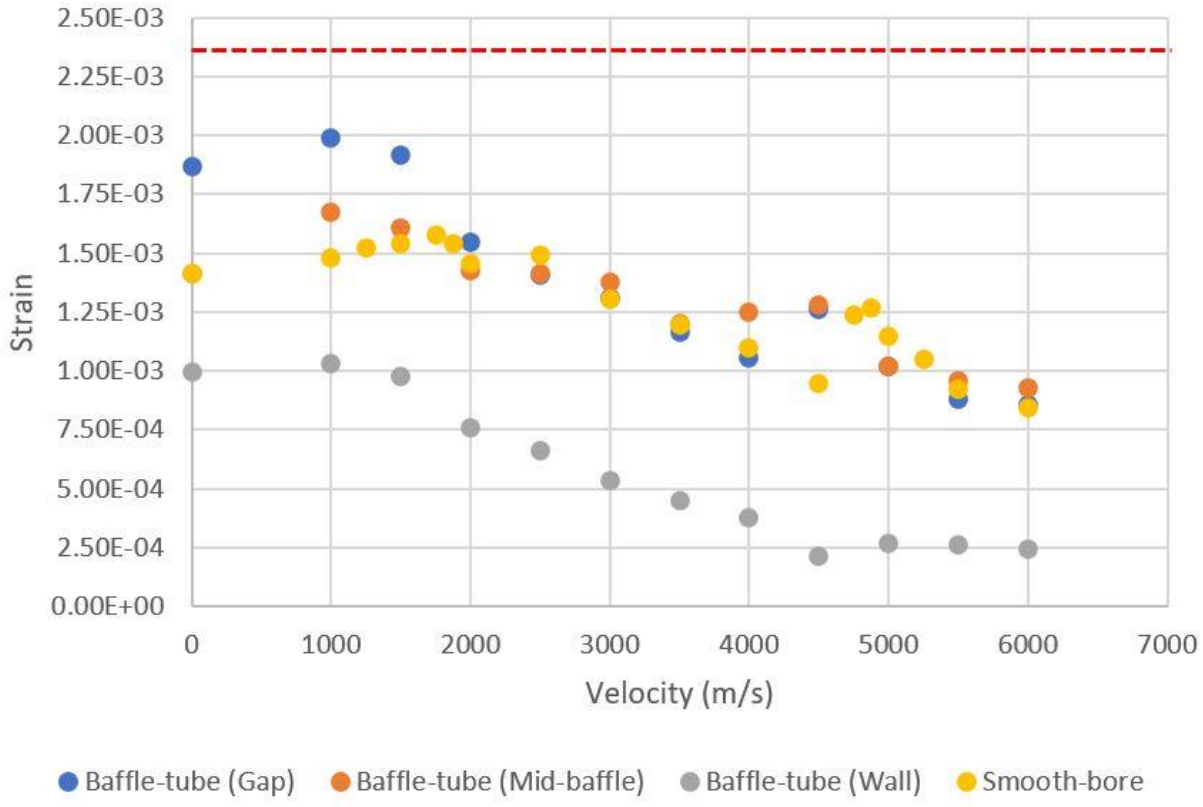

Figure 5.7: Combined smooth-bore and baffle-tube strain

5.3 Resonance

To find any resonance points within the ram accelerator system, three separate approaches were used. The first was frequency testing, this found fundamental frequencies at 792 Hz and 779 Hz for the smooth-bore and baffle-tube respectively. Unfortunately, variations in the waveform made measuring wavelengths difficult which in turn made correlating velocities and frequencies difficult, and this coupled with not knowing which harmonics would be excited by the applied pressure made the results of this simulation inconclusive.

The second approach was to look for peaks in the constant velocity test data. The initial data set did not show any resonance points for the baffle-tube, but two likely candidates for resonance points were visible in the smooth-bore data. Further simulation around these two potential locations in the smooth-bore configuration verified the existence of resonance effects which peaked at 1750 m/s and 4875 m/s, these points are visible in both the stress (Figure 5.1) and the strain (Figure 5.2).

The third and final approach to find resonance points was to use a constant acceleration simulation that ran between 1000 m/s and 6000 m/s. (As noted earlier, the initial velocity was 0 m/s, which allows for simulation of a larger range of velocities, because it shifted the locations of the velocities of interest, 1-6 km/s, away from the entrance of the tube where the boundary conditions caused error.) The results of the constant acceleration test, as seen in Figures 5.8 and 5.9, show a number of peaks, however these do not align with the resonance points found using the constant velocity data and further investigation shows them to be an artifact of the waveform, where the local maxima correspond to the maximum strain being tensile and the local minima correspond to compressive maximum strain. The constant acceleration data also has no noticeable reaction to the resonance points found through the constant velocity tests. This is not surprising

because resonance effects build up over time and the very high acceleration needed to accelerate the pressure wave from a standstill to 6000 m/s in 2 m of tube causes the wave to move through the areas of resonance very quickly.

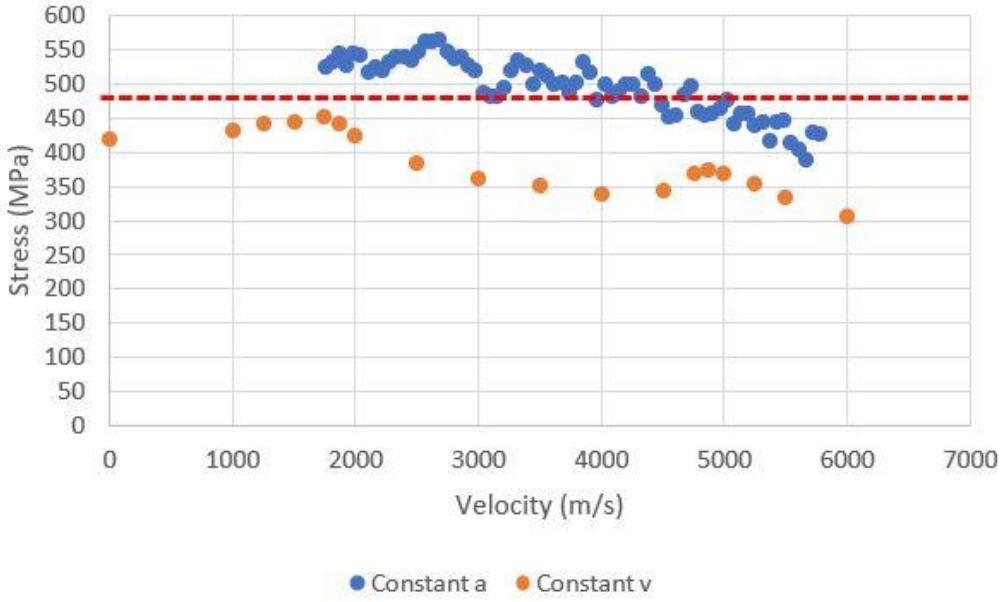

Figure 5.8: Smooth-bore combined constant v/a max stress

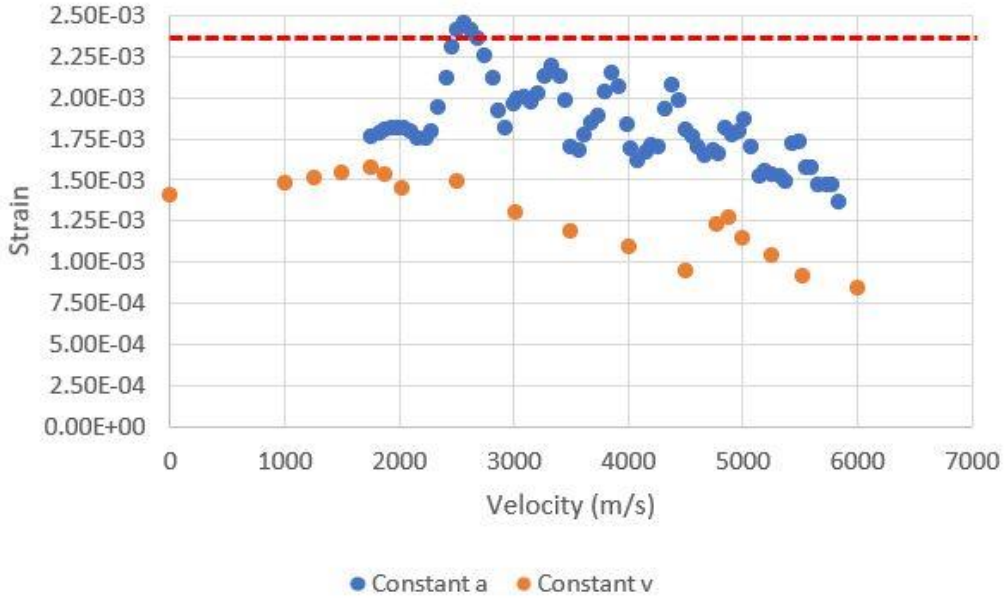

Figure 5.9: Smooth-bore combined constant v/a max strain

5.3.1 Resonance mitigation

The safest strategy for dealing with resonance is to design the system to avoid resonance frequencies entirely. However, the method of moving past resonance frequencies very quickly, as was demonstrated in the constant acceleration tests in Figures 5.8 and 5.9, is often the next best approach. When neither of these approaches are feasible and the system will be experiencing resonance frequencies for a relatively long duration, another approach that can be taken is to modify the structure itself to change the natural frequency, thus avoiding the resonance condition. In a ram accelerator, this approach would likely take the form of reinforcing certain sections of the barrel where the projectile will be at a velocity that corresponds to a resonance condition within the wall of the barrel. This reinforcement could take the form of replacing barrel sections to change material or geometry, fitting another tube around the outer surface of the barrel, or perhaps simplest, the relevant sections of the barrel could simply be wrapped with a fiber-reinforced composite.

Chapter 6

CONCLUSION

6.1 Conclusion

For this project, an FEA model of the ram accelerator barrel was developed to investigate the stress and strain response due to varied velocity, gaps in the inner surface of the barrel, and resonance induced by travelling projectile. Data collected from the FEA simulations showed that as projectile velocity increased both maximum stress and strain decreased, but they did not decrease equally, with the smooth-bore case showing a decrease in strain almost 1.5x greater than the decrease in stress. The gaps in the inner barrel surface caused a 17% and 13% increase in stress and strain respectively over the equivalent smooth-bore simulations. However, even with the exaggerated gap size, the pressure applied directly to the shell-tube never caused the shell-tube to experience a higher stress than was seen in the baffle. The constant velocity simulations showed that the smooth-bore configuration had two resonance points which amplified the stress and strain in their vicinities. Any ram accelerator system being tested should locate analogous resonance points and ensure the risks they pose are properly mitigated.

6.2 Prospectus

There are many directions in which this work could be expanded to better understand the ram accelerator barrel's response to the dynamic pressures of firing. One very valuable avenue of

research would be to experimentally validate this model by attaching strain gauges to the outside of the ram accelerator barrel during a shot and simulating the same system using this model. Comparing the simulation results to the experimental data would show the accuracy of the model, and could potentially provide insights into how the model might be altered to better fit the experimental data. Beyond experimental testing, there are any number of options for future work using the modelling framework set up here. Modifications to bore size, wall thickness, wave shape, or many other variables could be interesting subjects to study in the future. More complex geometries also be included, like modelling a more realistic baffle, or adding the barrel reinforcements discussed in the previous chapter to mitigate resonance conditions.

BIBLIOGRAPHY

[1] Hertzberg, A., Bruckner, A. P., and Bogdanoff, D. W., “Ram Accelerator: A New Chemical Method for Accelerating Projectiles to Ultrahigh Velocities,” AIAA Journal, Vol. 26, No. 2, 1988. doi:10.2514/3.9872, URL https://doi.org/10.2514/3.9872.

[2] Jones, H. W., "The Recent Large Reduction in Space Launch Cost," in *48th International Conference on Environmental Systems*, Albequerque, NM, 2018.

[3] Knowlen, C. and Bruckner, A. P., "Direct space launch using ram accelerator technology," *AIP Conf. Proc.*, Vol. 552, pp. 583-588, 2021.

[4] Correy, J., Leege, B. J., Bernhard, D., Ginos, J., Yancey, C., Knowlen, C., Higgins, A.J., "Investigation of Baffled-Tube Ram Accelerator Configurations" *AIAA SciTech Forum*, 2023. doi:10.2514/6.2023-2186, URL https://doi.org/10.2514/6.2023-2186

[5] MatWeb, "AISI 1060 Steel," [Online]. Available: https://www.matweb.com/search/datasheet.aspx?matguid=ecd1f5f21fe943e7a892d70ea57a43e8&ckck=1. [Accessed 12 08 2024].

[6] Daneshvaran, N., Leege, B. J., and Knowlen, C., "Computational Fluid Dynamic Modeling of Railed Tube Ram Accelerator in Reactive Flow," *AIAA SciTech Forum,* 2022. doi:10.2514/6.2022-2070, URL https://doi.org/10.2514/6.2022-2070

[7] Correy, J., Bernhard, D., Ginos, J., Knowlen, C., and Higgins, A. J., "Mach Number Effects on Baffled-Tube Ram Accelerators," in *AIAA SciTech Forum,* 2024. doi:10.2514/6.2024-1610, URL https://doi.org/10.2514/6.2024-1610

APPENDIX A

ABAQUS DLOAD File with Comments

```
      SUBROUTINE DLOAD(F,KSTEP,KINC,TIME,NOEL,NPT,LAYER,KSPT,
     1 COORDS,JLTYP,SNAME)
C
      INCLUDE 'ABA_PARAM.INC'
C
      DIMENSION TIME(2), COORDS (3)
      CHARACTER*80 SNAME

C   Everything above this line is standard and shouldn't be changed without good reason

            X=COORDS(1)
            Y=COORDS(2)
            Z=COORDS(3)

            Velocity = 1000
C           Standard pulse width of 10 us duration at 1000 m/s
            Pulse_width_us = 10
            Pulse_width = Pulse_width_us*(.000001)*1000
            Half_pulse = Pulse_width*.5
            Z_position = Velocity*TIME(2)

C           The variable (X,Y,Z) used in the next line depends on how the tube is modelled
C           The name Z_position is arbitrary and doesn't need to be changed for X or Y directions
            if (Y.le.(Z_position+Half_pulse).and.Y.ge.(Z_position-Half_pulse)) then
                  F_ksi = 50
                  F = F_ksi*6894757.293
            else
                  F = 0
            endif


      RETURN
      END
```

For constant acceleration cases, replace lines beginning with Velocity with

```
            Velocity = a*Time(2)+v_0
```

And the line beginning with Z_position with

```
            Z_position = .5*a*Time(2)*Time(2)+v_0*Time(2)
```

And add these lines above Velocity and fill in your values

a= acceleration here
v_0= initial velocity here

Everything between the if and endif commands defines the shape and amplitude of the pressure wave, the code for the 10 μs square wave is included here. This section of the code could easily be modified to create a more complex waveform, the waveform doesn't need to be symmetric as it is here, nor does the Z_position variable need to represent the middle of the wave.

In this code I didn't use any scientific notation nor any other exponents because including exponents caused some very strange behavior that I was never able to fix, though interestingly engineering notation seems to work.

To use this code in ABAQUS, make sure you use a Dynamic, Implicit step as DLOAD is only valid for the implicit solver. When you define a load, select the "User-defined" option and select all the surfaces the load will apply to. When you set up a job, in the general tab there is an option to attach a "user subroutine file", make sure your DLOAD file is in your working directory and select it here. The DLOAD file can be set up or edited in any text editor (word, notepad, notepad++, etc.) (notepad++ is ideal because it has a Fortran editor mode) but the file needs to be saved with the ".f" extension to be valid.